



The roles of Rh crystal phase and facet in syngas conversion to ethanol

Li Kang^{a,b,c,1}, Yuan Zhang^{a,b,1}, Lixuan Ma^{a,b}, Baojun Wang^{a,b,*}, Maohong Fan^{d,e,f}, Debao Li^g, Riguang Zhang^{a,b,*}



^aState Key Laboratory of Clean and Efficient Coal Utilization, Taiyuan University of Technology, Taiyuan 030024, Shanxi, PR China

^bKey Laboratory of Coal Science and Technology (Taiyuan University of Technology), Ministry of Education, PR China

^cKey Laboratory for Green Chemical Technology, School of Chemical Engineering and Technology, Tianjin University, Collaborative Innovation Center of Chemical Science and Engineering (Tianjin), Tianjin 300072, PR China

^dDepartments of Chemical and Petroleum Engineering, University of Wyoming, Laramie, WY 82071, USA

^eSchool of Civil and Environmental Engineering, Georgia Institute of Technology, Atlanta, GA 30332, USA

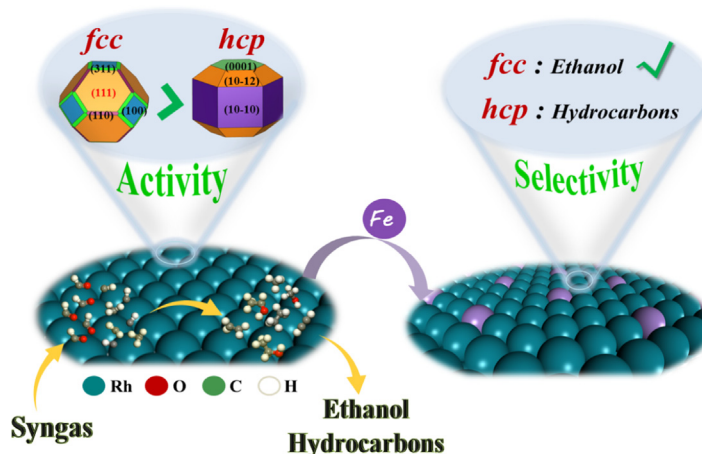
^fSchool of Energy Resources, University of Wyoming, Laramie, WY 82071, USA

^gState Key Laboratory of Coal Conversion, Institute of Coal Chemistry, Chinese Academy of Sciences, Taiyuan 030001, Shanxi, PR China

HIGHLIGHTS

- The effect of Rh crystal phase on the catalytic performance in syngas-to-ethanol is for the first time identified.
- The fcc Rh exposes much denser active facets compared to the hcp Rh.
- The fcc Rh exhibits higher intrinsic activity for CH and ethanol formation than the hcp Rh.
- Compared to Ni, Ru, Co and Cu, the fcc Rh realizes a balance between CH and undissociated CO/CHO.
- The fcc Rh is still superior to the hcp Rh for Fe-modified Rh-based catalysts.

GRAPHICAL ABSTRACT



ARTICLE INFO

Article history:

Received 27 January 2021

Received in revised form 5 October 2021

Accepted 5 October 2021

Available online 08 October 2021

Keywords:

Rh-based catalysts

Syngas

Ethanol

Crystal phase

Catalytic performance

ABSTRACT

Design of Rh catalyst by controlling crystal phase and facet is significant for providing higher mass-specific activity and selectivity for ethanol synthesis from syngas. We demonstrate here the roles of crystal phase and facet in syngas conversion to ethanol on different crystal facets of fcc and hcp Rh by DFT calculations and microkinetic modeling. Compared to hcp Rh, fcc Rh not only exhibits higher intrinsic activity for CH and ethanol formation, but also exposes much denser active facets and inhibits methanol, especially, the mainly exposed (111). Further, for the Fe-modified Rh catalysts, fcc Rh exhibits better activity and selectivity toward ethanol, which is still superior to hcp Rh. Thus, Rh-based catalysts should be focused on the fcc crystal phase instead of hcp crystal phase. The findings in this work are significantly beneficial to the rational design of Rh-based catalysts for CO hydrogenation to desired ethanol.

© 2021 Elsevier Ltd. All rights reserved.

1. Introduction

Hydrogenation of CO/CO₂ to high-value fuels and chemicals, such as ethanol, is one of the most promising methods for

* Corresponding authors.

E-mail addresses: wangbaojun@tyut.edu.cn, wbj@tyut.edu.cn (B. Wang), zhan-riguang@tyut.edu.cn (R. Zhang).

¹ Represents co-first authors, and contributed equally to this work.

utilization of the large amount of captured CO₂ (Farrell et al., 2006; Pan et al., 2007; An et al., 2019; Yang et al., 2019; Song et al., 2017). Nowadays, certain promoters and/or reducible metal oxides promoted-Rh catalysts (Spivey and Egbibi, 2007; Subramani and Gangwal, 2008; Luk et al., 2017) have been widely used for ethanol synthesis from CO hydrogenation, especially, the promoter (transition metals (Liu et al., 2013; Xie et al., 2016; Glezakou et al., 2012); alkalis metals (Schwartz et al., 2011; Yang et al., 2018); rare earth elements (Xu et al., 2017; Liu et al., 2016)-modified Rh-based bimetallic catalysts. So far, extensive experimental (Yang et al., 2017; Song et al., 2012; Liu et al., 2013; Xie et al., 2016; Glezakou et al., 2012) and theoretical (Liu et al., 2016; Li et al., 2012; Mei et al., 2010; Choi and Liu, 2009; Wang et al., 2014) studies on the Rh-based catalyst catalyzing CO hydrogenation have been exclusively focused on the face-centered-cubic (fcc) Rh. However, it is well known that different crystal structures, such as fcc and hexagonal-close-packed (hcp), will in general exhibit different catalytic performance. For example, the mechanism and activity of CO activation over the Ni (Liu et al., 2016); Ru (Li et al., 2017) and Co (Liu et al., 2013) catalysts strongly depend on the crystal phase. Recently, Huang et al. (Huang et al., 2017) discovered that hcp Rh can be synthesized in the form of nanoparticles because of lower surface energy of hcp Rh; moreover, the large lattice expansion in the hcp Rh structure may be used to tune the reactivity and/or selectivity of Rh-based catalysts.

Different crystal phases of metal catalyst correspond to different symmetries and expose various crystal facets, which further affect the catalytic performance toward the desired reactions (Liu et al., 2016; Li et al., 2017; Liu et al., 2013; Zhang et al., 2020; Kusada and Kitagawa, 2016; Liu and Li, 2016). CO hydrogenation to ethanol over the different crystal facets of fcc Rh has been intensively investigated, mainly focusing on Rh(100) (Li et al., 2012); Rh(111) (Choi and Liu, 2009; Yang and Liu, 2014; Yang et al., 2016; Kapur et al., 2010) and Rh(211) (Wang et al., 2014; Yang et al., 2016; Kapur et al., 2010; Medford et al., 2014) facets, suggesting that the crystal facets of fcc Rh catalysts not only affect the existence form of CH_x intermediates and the preferred pathway of ethanol formation, but also affect the catalytic performance. Nørskov et al. (Yang et al., 2016) experimentally and theoretically found that Rh(211) presents high selectivity toward methane, whereas Rh(111) is highly selective toward C₂ oxygenates.

There has been little research on CO hydrogenation to ethanol on hcp Rh. Hence, the performance of hcp Rh crystal facets for catalytic hydrogenation of CO to ethanol was unknown until this study. It has been shown that phase transitions between hcp and fcc may occur as a result of the catalyst size (Huang et al., 2017; Kitakami et al., 1997), varying the supports and promoters, and pretreating the catalysts (Liu et al., 2013; Fan and Zhang, 2016; Braconnier and Landrison, 2013; Prieto, 2013).

We apply density functional theory (DFT) calculations and microkinetic modeling to examine the mechanism of CO hydrogenation to ethanol over the different crystal facets of fcc and hcp Rh, as well as Fe-modified fcc and hcp Rh, in which both (111) and (100) facets with the surface proportion (as estimated from Wulff construction) of 66.95% and 14.83% for the fcc Rh, as well as (0001), (10-10) and (10-12) facets with the surface proportion of 45.34%, 37.74% and 16.92% for the hcp Rh are taken into account. The Wulff construction results used here were obtained by Huang et al. (2017). We also compare the key step of CO hydrogenation to ethanol on the Rh, Ni, Co, Ru and Cu. The comprehensive understanding of fcc and hcp Rh catalysts provide a pattern for illustrating the catalytic activity and selectivity of more complex Rh-based catalysts, and point the way for the experimental optimization and design of novel Rh-based catalysts in CO hydrogenation to ethanol.

2. Computational details

2.1. Computational models

According to the Wulff construction method, Huang et al. (Huang et al., 2017) have obtained the equilibrium crystal shapes of fcc Rh and hcp Rh, indicating that fcc Rh mainly contains the (111), (100), (311) and (110) crystal facets with the surface proportion of 66.95%, 14.83%, 11.86% and 6.36%, respectively. On the other hand, hcp Rh mainly contains the (10-10), (10-12) and (0001) crystal facets with the surface proportion of 45.34%, 37.74% and 16.92%, respectively. However, several researches have shown that Rh(100) exhibits high activity of CO activation (Li et al., 2012; Koster and Santen, 1990; Pilot et al., 2011), and the effect of fcc and hcp Rh crystal phases and facets on CO dissociation (Li et al., 2012) have revealed that the activity of CO dissociation over the fcc Rh depends on the (100) and (111) facets, while that over the hcp Rh depends on the (0001), (10-12), and (10-10) facets. Thus, both (111) and (100) facets with the total surface proportion of 81.78% for the fcc Rh, as well as the (0001), (10-10) and (10-12) facets with the surface proportion of 100% for the hcp Rh are considered in this study.

In the current work, the calculated lattice constants for the hcp Rh are $a = b = 2.767 \text{ \AA}$, $c = 4.276 \text{ \AA}$ and $a = b = c = 3.842 \text{ \AA}$ for the fcc Rh, which agree with the experimental values (Huang et al., 2017) of $a = b = 2.78 \text{ \AA}$, $c = 4.64 \text{ \AA}$ for the hcp Rh and $a = b = c = 3.88 \text{ \AA}$ for the fcc Rh, respectively. $p(3 \times 2)$ and $p(2 \times 3)$ supercell surfaces were used to model the (10-10) and (10-12) facets, respectively; the $p(3 \times 3)$ supercell surface was adopted to model the (111), (100) and (0001) facets (see Fig. 1). All these surfaces to model different Rh crystal facets are large enough to avoid the lateral interaction of adsorbates. The vacuum region of 15 Å was employed. In all calculations, the bottom two layers were fixed, and the other layers together with the adsorbed species were allowed to relax. The structure of the five Rh crystal facets is described in detail in the Supplementary Material. The dipole correction is not applied in this work on the basis of previous studies about syngas conversion to ethanol is investigated over Rh catalysts (Yang et al., 2017; Choi and Liu, 2009; Asundi et al., 2019; Gu et al., 2020); in which the dipole correction has not been considered, moreover, the obtained results can well clarify the reaction mechanism, and some results agree with the experimental fact. Further, the adsorption free energy and stable adsorption configurations of CH₃CH₂O on the different Rh facets are calculated using the dipole corrections, as listed in Table S2, the adsorption free energies of CH₃CH₂O with the dipole corrections are little affected compared to those without the dipole corrections, moreover, the change of the adsorption configurations is negligible.

2.2. Computational methods

All calculations in this study were conducted on the basis of periodic density functional theory (DFT) implemented in the Vienna Ab-initio Simulation Package (VASP) code (Furthmüller et al., 1996; Kresse and Furthmüller, 1996). The exchange-correlation functional was treated by the Perdew-Burke-Ernzerhof (PBE) of the generalized gradient approximation (GGA) (Perdew et al., 1996). The cutoff energy was set as 400 eV; and the Monkhorst-Pack grid size of (9 × 9 × 9) was used to calculate the lattice parameters. The optimization was thought to be converged when the forces on the ions are less than 0.01 eV/Å, and the change of total energy is converged to 5×10^{-6} eV/atom.

The surface Brillouin zone was sampled with a (3 × 3 × 1) Monkhorst-Pack grid for the Rh(111), (100) and (0001) facets, (4 × 4 × 1) for the Rh(10-10) facet, and (3 × 5 × 2) for the Rh

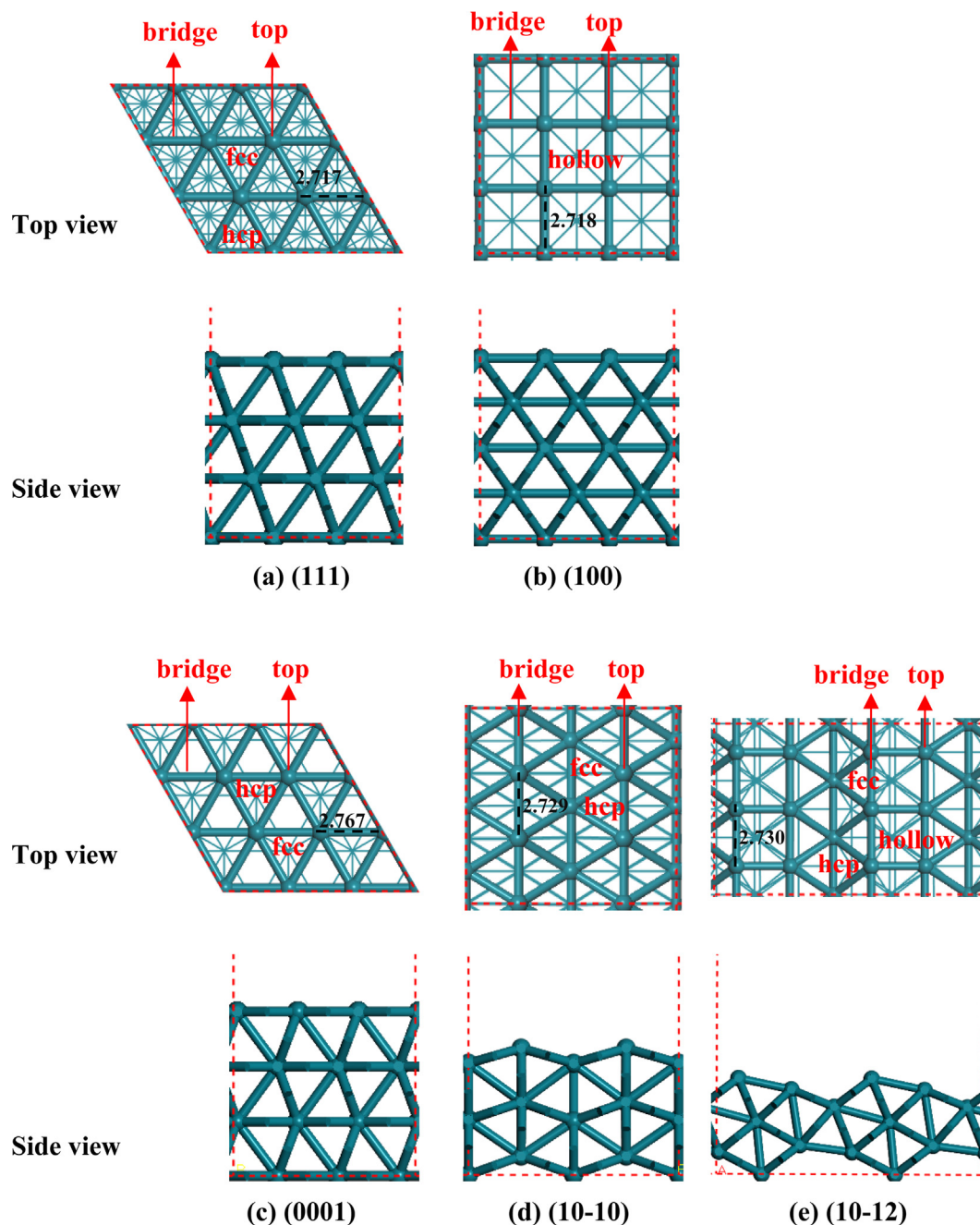


Fig. 1. The facet morphology and adsorption sites of (a) (111) and (b) (100) facets for the fcc Rh, (c) (0001), (d) (10-10), (e) (10-12) facets for the hcp Rh.

(10-12) facet. The climbing-image nudged elastic band (CI-NEB) and dimer methods were used to identify transition state (TS) structure (Henkelman et al., 2000; Henkelman and Jónsson, 2000; Henkelman and Jónsson, 1999). Finally, the TS structure is verified by the frequency analysis, which corresponds to only one imaginary frequency, as listed in Table S3. Further, since CO hydrogenation to ethanol usually occur at the temperature range of 500–623 K (Glezakou et al., 2012; Yin et al., 2003), all energies are calculated at 523 K in this study (see details in the [Supplementary Material](#)).

3. Results and discussion

It is widely accepted that CO hydrogenation to ethanol involves two key steps (Pan et al., 2007; Li et al., 2012; Kapur et al., 2010;

Zuo et al., 2014; Zhao et al., 2011; Zhang et al., 2014). The first step is the formation of key CH_x intermediates by either CO direct dissociation followed by C successive hydrogenation, or CO H-assisted dissociation via the C-O bond breakage of CH_xO or CH_{x-1}OH ($x = 1-3$); methanol may be formed by CH_xO or CH_{x-1}OH ($x = 1-3$) hydrogenation to affect the selectivity and production of the primary CH_x intermediate. The second step is the C-C bond formation of C_2 oxygenates via CHO or CO reaction with the primary CH_x intermediates to form CH_xCHO or CH_xCO , and subsequent successive hydrogenation to ethanol; the hydrocarbons formed by CH_x ($x = 1-3$) hydrogenation or coupling probably affect the selectivity and production of ethanol. In this study, we examine the reactions involving CO activation, the formation of CH_x and methanol, as well as the formation of ethanol and hydrocarbons (methane and C_2 hydrocarbons) on the (111), (100) facets of fcc

Rh and (0001), (10–10), (10–12) facets of hcp Rh at 523 K (Table 1, see details in the Supplementary Material).

3.1. The effects of Rh crystal phase and facet on CO activation, CH_x and methanol

For CO activation, our results show that for both fcc and hcp Rh, CO direct dissociation is a significantly higher energy pathway compared to CO hydrogenation to CHO or COH (see Figs. S6 and S7); moreover, CHO formation is more favorable than COH formation, which agrees with previous results on Rh(111) (Choi and Liu, 2009; Yang and Liu, 2014; Yang et al., 2016; Kapur et al., 2010). We find that both fcc Rh(100) and hcp Rh(10–10) facets are the most active, in agreement with previous studies showing that Rh(100) exhibits high activity for CO activation (Koster and Santen, 1990; Filot et al., 2011). Thus, the activity of CO activation is sensitive to Rh crystal facet; CHO will be the major intermediate leading to the formation of CH_x and methanol.

Based on the previous studies (Choi and Liu, 2009; Wang et al., 2014; Yang et al., 2016; Zhang et al., 2014; Zhang et al., 2013; Wang et al., 2018; Zhang et al., 2013; Zheng et al., 2015); the possible formation pathways of CH_x ($x = 1-3$) and methanol over the (111), (100) facets of fcc Rh and (0001), (10–10), (10–12) facets of hcp Rh are considered in this study (see details in Figs. S8–S14). The results show that the CH monomer is formed both thermodynamically and kinetically favored over the CH₂ and CH₃ monomers (see Fig. S9), suggesting that the CH monomer is the most abundant CH_x species over the five Rh crystal facets studied here, which mainly comes from the C–O bond breakage of CHO or/and COH

intermediates. However, the favorable formation pathway of CH monomer depends on the structure of crystal facet, as shown in Fig. S9, the dissociation of CHO and COH are two competitive pathways for CH formation on the Rh(0001) and (10–10) facets; CHO dissociation is more favorable for CH formation on the Rh(10–12) and (100) facets; COH dissociation mainly contribute to CH formation on Rh(111) facet. Moreover, the activity of CH formation is also affected by Rh crystal facet and phase, as shown in Fig. 2(a), among five Rh facets, Rh(100) exhibits the highest activity for CH formation with the smallest overall free energy barrier of 196.7 kJ·mol⁻¹. The reason for the low barrier is attributed to that Rh(100) facet is composed of 4-fold flatted sites that favor C–O bond breakage of CHO, and the identical conclusions were also obtained for Ru (Li et al., 2017) and Cu (Zheng et al., 2015) catalysts. More importantly; the overall free energy barriers of CH formation over the (111) and (100) facets of fcc Rh are lower than those over the (0001), (10–10) and (10–12) facets of hcp Rh. On the other hand, among the five Rh facets, CH formation is much easier in kinetics than methanol formation over the (111), (100), (0001) and (10–12) facets; methanol formation is energetically competitive with CH formation only on the (10–10) facet. Taking the intermediate coverage in the process of CH formation into consideration, microkinetic modeling (Choi and Liu, 2009) (see details in the Supplementary Material) is employed to quantitatively calculate the formation rate of the favored CH monomer and CO hydrogenation to methanol under the typical conditions ($P_{CO} = 4$ atm, $P_{H_2} = 8$ atm; $T = 523$ K). Considering the complexity of the reaction system in this study and the computational cost, microkinetic modeling assumes that there are no interactions between the

Table 1
Activation free energy (G_a) and reaction free energy (ΔG) involving in CO hydrogenation to ethanol over the Rh(111), (100), (0001), (10–10) and (10–12) facets at 523 K.

Reactions		$G_a(\Delta G)$ (kJ·mol ⁻¹)				
		(111)	(100)	(0001)	(10–10)	(10–12)
R1	CO → C + O	343.2(130.8)	210.1(63.2)	262.3(108.5)	317.6(183.7)	252.4(94.1)
R2	CO + H → COH	161.6(83.6)	159.1(65.5)	160.9(78.6)	126.5(59.0)	195.6(108.9)
R3	CO + H → CHO	139.9(117.3)	118.9(80.2)	149.1(119.8)	110.7(79.5)	147.0(106.0)
R4	CHO → CH + O	134.8(–10.6)	116.5(6.0)	118.0(–32.6)	150.2(15.3)	143.4(–3.4)
R5	CHO + H → COH	105.0(44.4)	102.1(59.5)	104.2(51.5)	95.0(49.0)	153.6(42.5)
R6	COH → CH + OH	64.2(–24.7)	113.0(–71.0)	67.8(–54.2)	102.6(–27.1)	121.0(–58.6)
R7	CHO + H → CH ₂ O	80.9(61.1)	78.1(59.2)	94.4(76.1)	68.0(61.1)	78.7(60.2)
R8	CH ₂ O → CH ₂ + O	105.1(–15.1)	107.1(22.3)	105.4(–41.7)	173.1(13.1)	150.9(0.7)
R9	CH ₂ O + H → CH ₂ OH	81.4(30.4)	91.6(45.9)	85.8(32.7)	78.9(10.1)	101.9(22.4)
R10	CH ₂ OH → CH ₂ + OH	81.7(–14.0)	87.6(–42.6)	76.6(–37.2)	91.2(–3.7)	64.7(–46.0)
R11	CH ₂ O + H → CH ₃ O	60.8(13.9)	93.6(35.2)	79.2(3.9)	43.3(–9.4)	77.0(15.6)
R12	CH ₃ O → CH ₃ + O	129.8(–11.4)	136.6(–11.1)	129.1(–9.9)	158.4(1.1)	164.9(–4.8)
R13	CH ₃ O + H → CH ₃ OH	70.5(15.4)	88.9(12.3)	95.9(23.1)	86.4(12.1)	129.7(51.9)
R14	C + H → CH	62.4(–40.1)	68.1(–26.2)	74.3(–26.9)	60.0(–60.2)	79.9(0.9)
R15	CH + H → CH ₂	49.3(37.1)	82.4(61.5)	69.2(54.1)	61.0(6.3)	92.4(56.1)
R16	CH ₂ + H → CH ₃	58.4(–1.7)	62.4(–13.6)	82.2(12.8)	37.5(–34.3)	49.1(8.6)
R17	CH ₃ + H → CH ₄	53.9(–44.6)	47.8(–53.8)	63.2(–27.0)	23.9(–63.4)	64.2(11.4)
R18	CH + CO → CHCO	133.6(94.8)	145.3(109.4)	143.9(122.9)	94.8(77.2)	146.5(100.2)
R19	CH + CHO → CHCHO	71.1(–0.8)	151.8(89.0)	89.0(40.2)	112.1(83.3)	142.5(–4.4)
R20	CH + CH → C ₂ H ₂	97.9(10.3)	156.7(13.7)	105.2(38.3)	104.3(–13.3)	158.4(–21.5)
R21	CH ₂ + CO → CH ₂ CO	129.3(86.9)	114.9(26.8)	162.0(63.4)	80.6(41.0)	121.0(64.6)
R22	CH ₂ + CHO → CH ₂ CHO	72.5(–32.3)	141.1(–18.4)	76.6(–0.9)	64.7(–66.3)	132.2(–13.4)
R23	CH ₂ + CH ₂ → C ₂ H ₄	86.7(–62.6)	125.2(–65.6)	114.4(–43.0)	65.5(–83.5)	86.3(–52.0)
R24	CH ₃ + CO → CH ₃ CO	149.0(21.5)	133.1(14.0)	155.2(25.2)	128.1(11.9)	137.0(26.5)
R25	CH ₃ + CHO → CH ₃ CHO	84.8(–61.7)	98.1(–7.1)	94.9(–29.6)	50.7(–45.3)	106.9(24.7)
R26	CH ₃ + CH ₃ → C ₂ H ₆	139.1(–75.1)	116.1(–112.5)	114.3(–75.8)	174.6(–42.0)	203.1(–49.0)
R27	CHCO + H → CH ₂ CO	–	107.5(16.1)	–	–	97.2(10.2)
R28	CHCO + H → CHCHO	–	86.3(76.3)	–	–	–
R29	CHCO + H → CHCOH	–	91.5(2.5)	–	–	88.7(–24.3)
R30	CHCHO + H → CH ₂ CHO	49.9(–2.2)	66.0(–59.5)	59.2(24.1)	–	47.0(–24.0)
R31	CHCHO + H → CHCHOH	82.5(26.8)	90.1(–8.2)	102.7(31.2)	–	97.5(24.5)
R32	CH ₂ CHO + H → CH ₃ CHO	62.6(–23.2)	61.3(7.8)	64.9(0.7)	–	69.1(24.4)
R33	CH ₂ CHO + H → CH ₂ CHOH	76.3(32.8)	93.5(28.0)	86.6(22.1)	–	80.4(12.1)
R34	CH ₃ CHO + H → CH ₃ CH ₂ O	57.2(–14.2)	48.3(–9.1)	69.6(0.2)	54.4(–5.3)	53.5(–3.0)
R35	CH ₃ CHO + H → CH ₃ CHOH	81.8(1.7)	92.6(8.9)	89.4(7.5)	89.0(–7.4)	107.4(–18.4)
R36	CH ₃ CH ₂ O + H → C ₂ H ₅ OH	79.7(–30.4)	110.2(10.9)	60.0(–13.8)	99.5(–6.2)	67.1(–22.2)

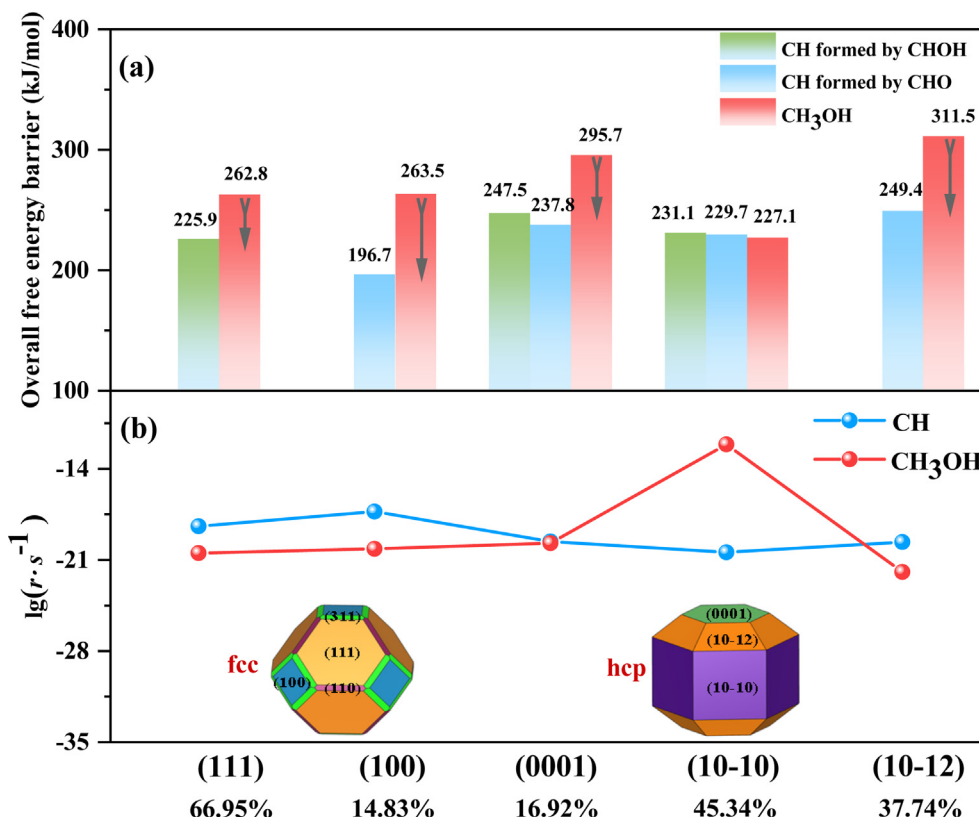


Fig. 2. (a) The overall free energy barrier and (b) the reaction rate for the favorable pathway of CH and methanol formation with respect to CO + H species over different crystal facets of fcc and hcp Rh. The arrows in (a) represent the deviations between overall free energy barrier gap for methanol and CH formation.

adsorbate-adsorbate based on the mean-field theory. In fact, for the high-coverage system, the coverage effect becomes highly complex and cannot be ignored, for example, previous studies about the coverage-dependent kinetic model (Yang et al., 2016; Lausche et al., 2013; Yao et al., 2019; Li and Sholl, 2015; Van Belleghem et al., 2016) showed that the adsorbate-adsorbate interactions have a great influence on the activity and products selectivity in the FTS reaction. Yang et al. (Yang et al., 2016) indicated that the high CO coverage decreases the adsorption of the intermediate and the stability of transition state on the Rh catalyst, especially the C-O bond cleavage in CHOH, reducing the activation energy to improve the reaction activity. Further, to confirm that the adsorbate-adsorbate interaction is the dominant reason for the deviation between our calculation and the literature (Yang et al., 2016), the adsorption free energy of CO is decreased to -0.98 eV based on the previous studies by Yang et al. (Yang et al., 2016), suggesting that when the adsorption free energy of CO is -0.98 eV, the coverage of CO reaches equilibrium (0.55 ML) at 523 K on Rh(111) facet, which can model the high coverage of CO under the realistic conditions on Rh(111) facet, as a result, the formation rates of CH and CH₃OH are 1.27×10^{-8} and $5.00 \times 10^{-12} \text{ s}^{-1}$, respectively, which are close to the results in the literature (Yang et al., 2016). Thus, although the agreement between the microkinetic modeling in this work and the previously reported values is only semi-quantitative, the results can provide strong support for the structure-sensitive of Rh crystal phase and crystal facets; in addition, the effect of the adsorbate-adsorbate interactions on the reaction activity and product selectivity will be considered in our future work. Additionally, given that CH species as the intermediate has poor stability, methane formation rate is employed as an indicator for the extent of CH formation, as well as methanol as the reference in the microkinetic

modeling, to study the effect of crystal Rh crystal phases and facets on the methane (CH*) and methanol formation under the typical conditions.

As indicated in Fig. 2(b), the rate of CH formation is the fastest on the (100) facet, followed by the (111), (0001), (10-12) and (10-10) facets, which agrees with that obtained by the overall free energy barrier, that is, among five Rh facets, the fcc Rh(100) facet has the highest intrinsic activity for CH formation. Further, CH formation rate over the (100) and (111) facets for the fcc Rh is higher by 1–3 orders of magnitude than those over the (10-10), (0001) and (10-12) facets for the hcp Rh. This implies that the fcc Rh catalyst overall exhibits higher intrinsic activity toward CH formation than the hcp Rh catalyst. Thus, the intrinsic activity of CH formation during CO hydrogenation on Rh catalyst is affected by the crystal phase and facet.

Additionally, the degree of rate control (DRC) of each elementary step is applied to measure the contribution of each elementary reaction to the product formation rate and confirmed the rate-controlled steps (Stegemann et al., 2009; Kozuch and Shaik, 2006) on the fcc Rh(111) and (100) facets. The values of DRC can be calculated using the following equation (Wang and Wang, 2021):

$$\text{DRC}_{i,j} = \frac{d(\ln R_j)}{d(\ln A_i)} = \frac{A_i dR_j}{R_j dA_i}$$

where R_j is the formation rate of product j , A_i is the pre-exponential factor of elementary reaction i . According to above equation, the DRC of the pre-referential factor response of each elementary step to the formation rate can be obtained (see Fig. 3). A positive value means the promoting effects of the elementary reaction on the product formation; a negative value means the inhibitory effects of the elementary reaction to the product formation. As shown in Fig. 3(a)

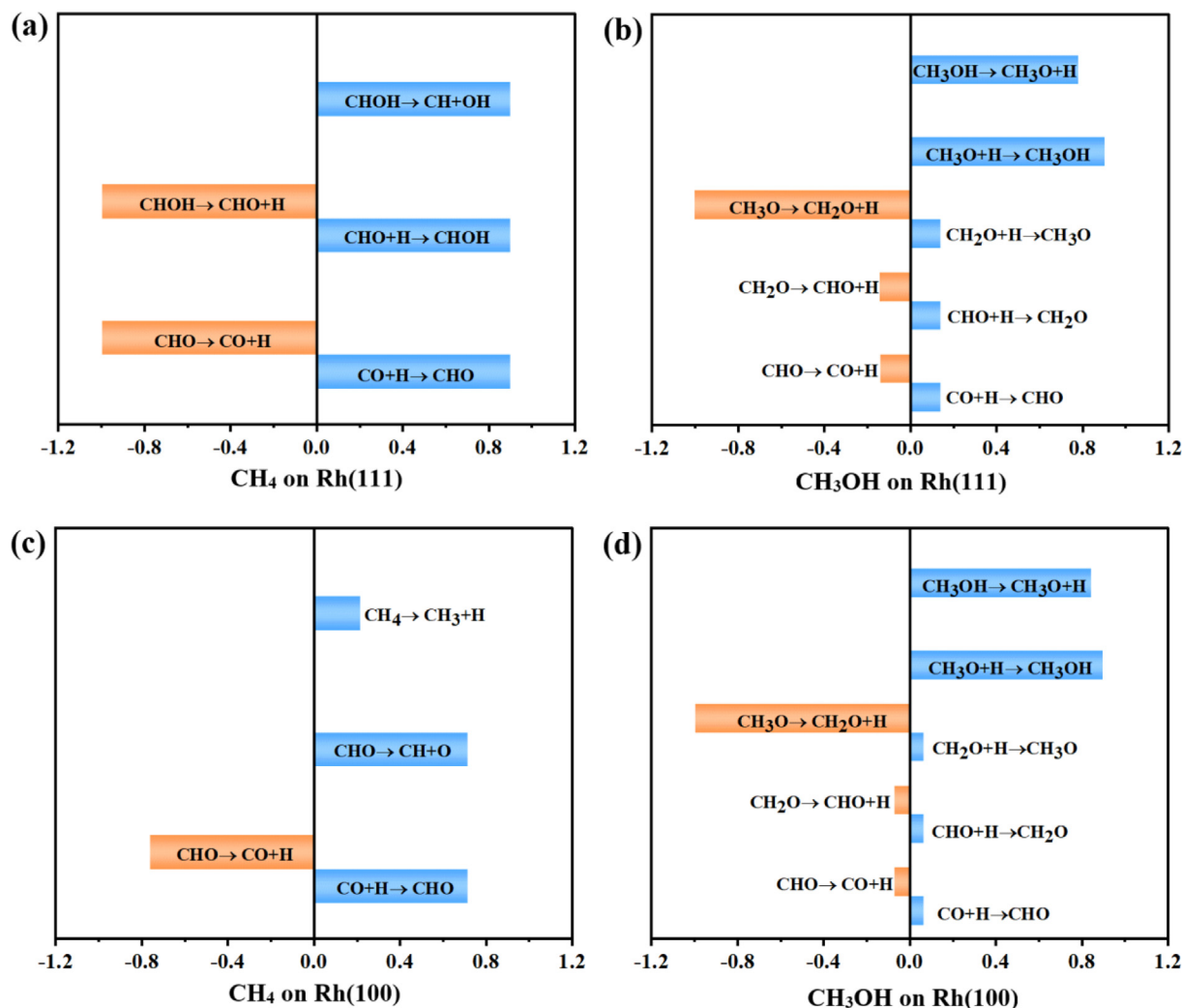


Fig. 3. DRC distribution of the elementary steps in the formation of methane and methanol on (a-b) Rh(111) and (c-d) Rh(100) facets, respectively. Only the reactions with DRC values greater than 0.05 are shown. +/- refer to positive or negative values of the DRC, which correspond to the promoting or inhibitory effects on the formation rate of methane and methanol.

and (b), on Rh(111) facet, the reactions related to CHOH formation and CHOH dissociation to CH are of great importance for methane formation rate; the reactions related to CH₃O hydrogenation to CH₃OH are critical for methanol formation rate. As shown in the Fig. 3 (c) and (d), on Rh(100) facet, the reactions related to CHO formation and CHO dissociation to CH are vital for methane formation rate; similar to Rh(111), the reactions related to the CH₃O hydrogenation to CH₃OH are significant for methanol formation rate.

On the other hand, CH formation is more favorable than methanol over (10–12) facet occupying 37.74% of the hcp Rh surface, and over the (100) and (111) facets occupying 81.78% of the fcc Rh surface (see Fig. 2(b)). In contrast, on (10–10) facet occupying 45.34% of the hcp Rh surface, the formation rate of methanol is higher than that of CH; on (0001) facet occupying 16.92% of the hcp Rh surface, the formation rate of methanol is equal to that of CH. Overall, based on the occupied proportion of different crystal facets in the hcp and fcc Rh crystal phases, the fcc Rh inhibits methanol formation and exhibits high activity of CH production, however, for the hcp Rh, only one third of the crystal facets show high CH selectivity.

Thus, the higher selectivity and intrinsic activity of fcc Rh for CO activation to form the primary CH monomer instead of methanol is verified from the formation of various favorable active facets not available for the hcp Rh, due to their different crystallographic

symmetries. The fcc Rh has a morphology effect distinct from that of hcp Rh, allowing fcc Rh to expose much denser active facets to effectively inhibit methanol formation and produce more CH species to take part in the subsequent C-C bond formation.

3.2. Comparisons of CH formation among the metals Rh, Ni, Co, Ru, Cu

CH monomer is the primary CH_x species on the different crystal facets of hcp and fcc Rh. Meanwhile, CH monomer is also a key intermediate in CO methanation on Ni (Liu et al., 2016; Zhi et al., 2015; Zhi et al., 2017) and in the FTS reaction on the Ru (Li et al., 2017; Liu and Hu, 2002; Filot et al., 2014) and Co (Liu et al., 2013; Yao et al., 2019; Zhang et al., 2016; Wen et al., 2016; Chen et al., 2016). Thus, the behavior of CO activation to form CH species is compared among the Ni, Co, Ru, Cu and Rh catalysts.

On the one hand, the activity of CO activation toward CH species is dependent on the metal. The overall free energy barrier of CH formation is 196.7 kJ·mol⁻¹ on the fcc Rh(100), which is much higher than that over the Ni (Liu et al., 2016); Ru (Li et al., 2017) and Co (Liu et al., 2013) catalysts (152.4, 90.7 and 103.2 kJ·mol⁻¹, respectively). On the Cu catalyst, the formation of CH_x is difficult to occur by the breakage of C–O bond in the CH_{x-1}OH or CH_xO (x = 1–3) intermediate, which is mainly hydrogenated to methanol (Zhang et al., 2013); However, CH_x formation is easier than metha-

nol over the Ni (Zhi et al., 2015; Zhi et al., 2017); Ru (Filot et al., 2014), Co (Wen et al., 2016; Chen et al., 2016) and Rh. These results show that Rh catalyst exhibits a lower activity for CH formation compared to the Ni, Ru and Co catalysts, and a higher activity compared to Cu catalyst. As shown in Fig. 4(a), Rh exhibits a moderate activity toward CH formation among the five types of metals, and contributes to the presence of the matched amount of CH_x and undissociated CO/CHO on Rh catalyst and facilitates the formation of C_2 oxygenates via the undissociated CO/CHO insertion into CH_x , thereby favoring ethanol formation. In contrast, the higher activity of CH_x formation on the Ni, Ru and Co catalysts lead to the majority of CO activation to form the abundant CH_x species, which in turn results in CH_x self-coupling or hydrogenation to form C_2 hydrocarbons or methane due to the absence of the undissociated CO/CHO species. On Cu catalyst, since CO is dominantly hydrogenated to form methanol and it is difficult to be activated to form CH_x species, C_2 oxygenates cannot be formed by CO/CHO insertion into CH_x species due to the lack of CH_x species.

On the other hand, the thermodynamics of the relevant reactions are also closely related to the type of metal catalysts. On the Rh catalyst, most of hydrogenation reactions are strongly endothermic, while the dissociation reactions are exothermic.

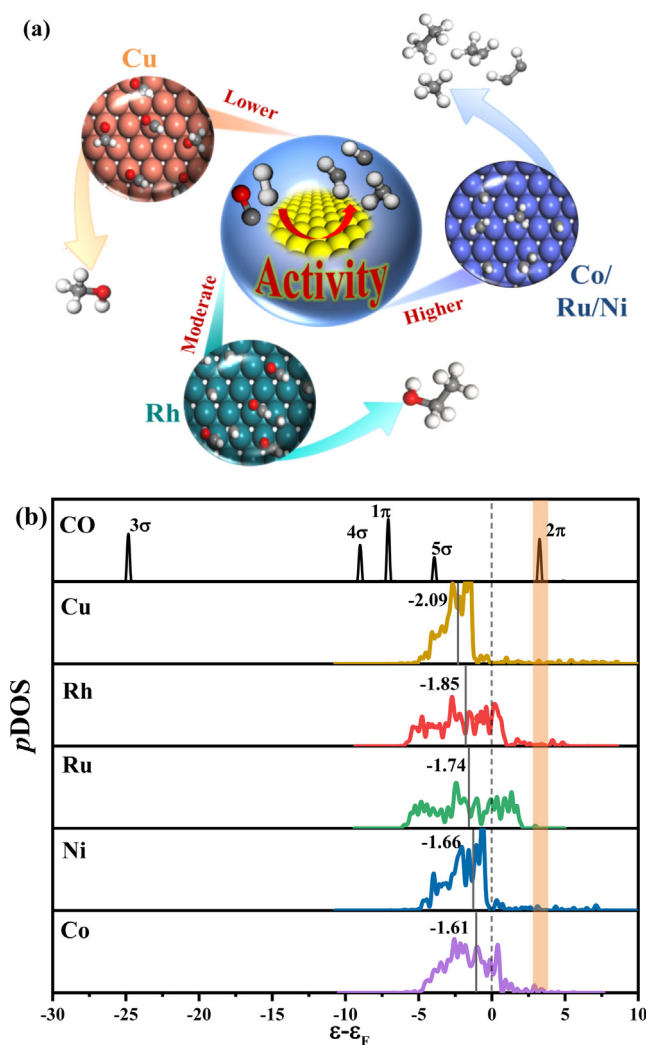


Fig. 4. (a) The product distribution of CO hydrogenation over the metals Rh, Ni, Co, Ru, Cu depending on the activity of CH_x formation, (b) Electronic densities of states (DOS) projected onto the molecule orbital of CO and d orbital of metal atoms on the Cu(111), Rh(111), Ru(111), Ni(111) and Co(111). The lower, moderate, and higher in (a) represent the relative activity of CH_x formation on five types metal catalysts.

Accordingly, CHO hydrogenation is thermodynamically difficult to form CH_xO and CH_xOH , as a result, methanol formation is inhibited and the primary CH monomer formation is promoted over Rh catalyst. Similar to Rh catalyst, on the Co (Liu et al., 2013; Yao et al., 2019; Zhang et al., 2016; Wen et al., 2016; Chen et al., 2016) and Ni (Zhi et al., 2015; Zhi et al., 2017) catalysts, the C-O bond cleavage of CO, CH_xO and CH_xOH are exothermic, the hydrogenation reactions are endothermic, thus, the CHO intermediate is thermodynamically inclined to the cleavage of C-O bond to form CH, and inhibit CO successive hydrogenation to methanol over the Co, Ni and Rh catalysts. In contrast, on the Cu catalyst (Koster and Santen, 1990; Zuo et al., 2014; Zhang et al., 2013; Wang et al., 2018), CO hydrogenation to methanol via the CHO, CH_2O and CH_3O intermediates is mostly exothermic, while the reactions related to the C-O bond breakage of CH_xO are endothermic, suggesting that Cu catalyst is thermodynamically conducive to CO successive hydrogenation to produce methanol and it is difficult to break the C-O bond of CH_xO and CH_xOH intermediates to form CH_x species.

To achieve a better understanding for the influence of metal catalyst type on CO activation to CH, the electronic properties analysis were carried out for CO adsorbed on the Cu(111), Rh(111), Ru(111), Ni(111) and Co(111) facets. Several excellent reviews (Van Santen and Neurock, 1995; Hammer and Nørskov, 2000) showed that CO adsorption on metal surface is mainly attributed to the interaction between the 5δ (HOMO) and 2π (LUMO) orbitals of CO molecule and the d orbitals of metal atom, especially, the back-donation from metal d orbitals to CO 2π antibonding orbitals will weaken the C-O bond. As shown in Fig. 4(b), depending on the number of electrons filled in the d orbital, the position d -band center related to Fermi level decreases in the order of $\text{Cu} > \text{Rh} > \text{Ru} > \text{Ni} > \text{Co}$, which agrees with the previous studies (Hammer and Nørskov, 2000). The d -band center of Co close to Fermi level readily back-donate the electrons to CO 2π antibonding orbital, contributing to the C-O bond activation. Additionally, the variation of the energy gap between HOMO and LUMO, the C-O bond length and the numbers of donated electrons for CO molecule before and after adsorbed on the Rh(111), Ru(111), Ni(111) and Co(111) facets are all more remarkable compared to Cu(111) facets (see details in Fig. S21 and Table S14). These results further confirmed that the adsorption behavior of CO on different metal catalysts could affect CH formation activity.

Above results confirm that compared to the Ni, Ru, Co and Cu catalysts, the Rh catalyst produces a balance between the amount of CH_x species and the undissociated CO/CHO. This is due to the catalyst's moderate activity toward CH_x formation. Having a balance of these species is necessary for CO hydrogenation to ethanol via C_2 oxygenates formation via the undissociated CO/CHO insertion into CH_x . The moderate activity of Rh gives a reasonable explanation for its success in the ethanol synthesis from syngas.

3.3. The effects of Rh crystal phase and facet on ethanol, methane and C_2 hydrocarbons formation

Previous studies (Li et al., 2012; Zhao et al., 2011; Zhang et al., 2014; Wang et al., 2018) found that three types of reactions can take place once the primary CH_x monomer is formed: the hydrogenation of CH_x to methane, the coupling of CH_x to C_2 hydrocarbons, and CO/CHO reaction with CH_x to C_2 oxygenates. Although CH is the primary CH_x monomer, CH_2 and CH_3 can be formed by CH successive hydrogenation; thus, the related reactions of CH, CH_2 and CH_3 species to produce methane, C_2 hydrocarbons and ethanol are further considered (see details in Figs. S15-S19), respectively.

As shown in Fig. 5(a), with respect to CH + CHO species, the most favorable pathway of ethanol formation is $\text{CH} + \text{CHO} + (\text{H}) \rightarrow \text{CHCHO} + \text{H} \rightarrow \text{CH}_2\text{CHO} + \text{H} \rightarrow \text{CH}_3\text{CHO} + \text{H} \rightarrow \text{CH}_3\text{CH}_2\text{O} + \text{H} \rightarrow \text{C}_2\text{H}_5-$

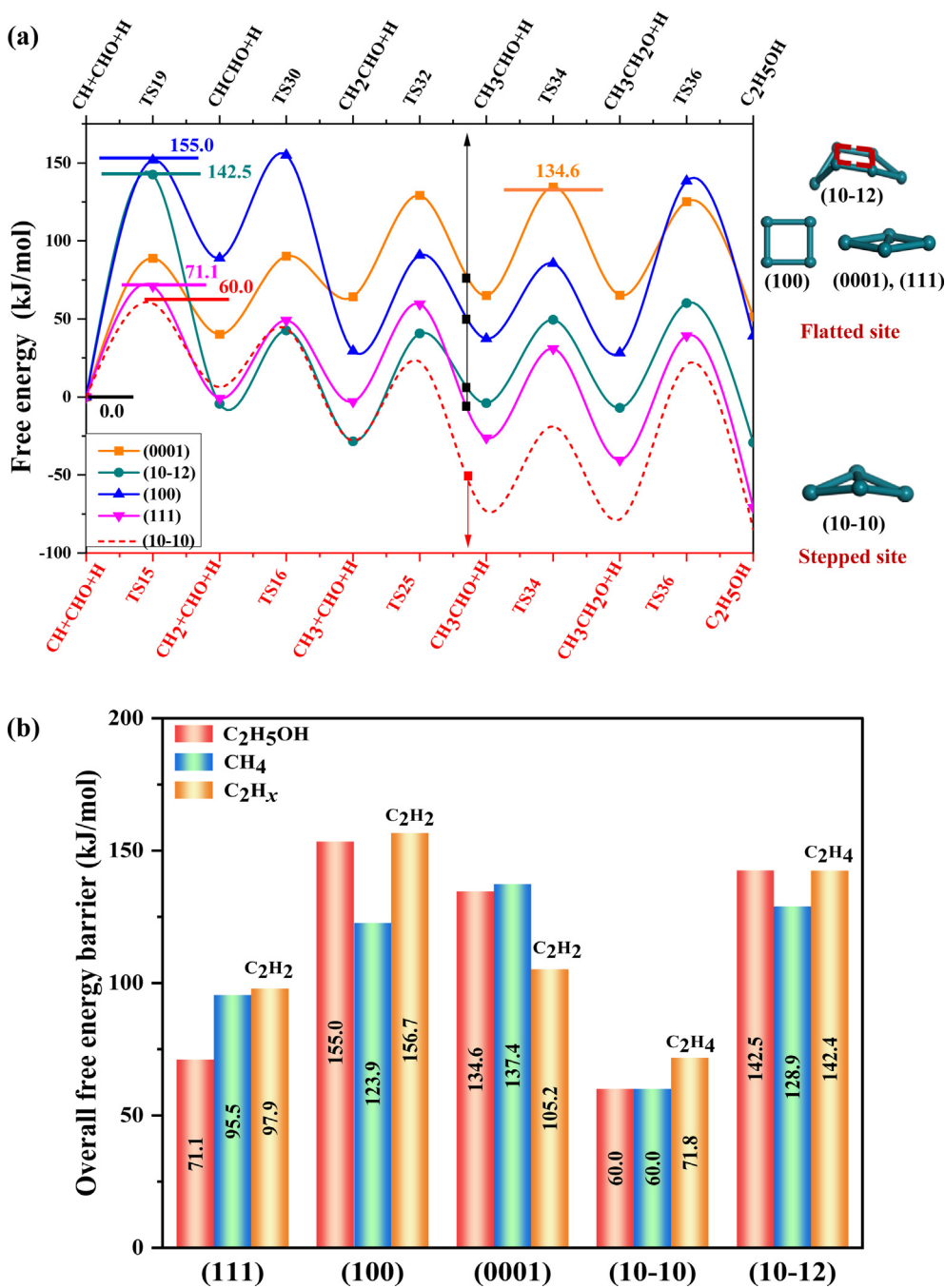


Fig. 5. (a) The free energy profiles of the most favorable pathway for ethanol formation with respect to CH + CHO species, (b) the comparison for the overall free energy barriers of the favorable pathway between ethanol and hydrocarbons on different crystal facets of fcc and hcp Rh at 523 K. The clusters in the right of (a) represent the structure features of the reaction sites on the corresponding Rh facets.

OH, which has the overall free energy barriers of 71.1, 155.0, 134.6 and 142.5 $\text{kJ}\cdot\text{mol}^{-1}$ over the (111), (100), (0001) and (10-12) facets, respectively. In contrast, on Rh(10-10) facet, CH is easily hydrogenated to form CH₃, then, CHO insertion into CH₃ produces C₂ oxygenates, the pathway of ethanol formation is CH+(CHO) + H → CH₂+(CHO) + H → CH₃ + CHO+(H) → CH₃CHO + H → CH₃CH₂-O + H → C₂H₅OH with the overall free energy barrier of 60.0 $\text{kJ}\cdot\text{mol}^{-1}$. Thus, the activity of ethanol formation over Rh catalyst also depends on the structure of crystal facet and corresponding reaction site, for example, the stepped Rh(10-10) facet presents a higher activity since all reactions related to ethanol formation mainly occur at the stepped sites; however, the stepped Rh(10-12) facet has a relatively lower activity, which is attributed to

that the related reactions preferentially occurred at the flatted sites instead of the stepped sites.

As presented in Fig. 5(b), for methane formation, the overall free energy barriers of 95.5, 123.9, 137.4, 60.0 and 128.9 $\text{kJ}\cdot\text{mol}^{-1}$ are required over the (111), (100), (0001), (10-10) and (10-12) facets, respectively. For C₂ hydrocarbons formation, CH self-coupling to C₂H₂ is favored over the (111), (100) and (0001) facets with the overall free energy barriers of 97.9, 156.7 and 105.2 $\text{kJ}\cdot\text{mol}^{-1}$, respectively; CH₂ self-coupling to C₂H₄ is the most favored over the (10-10) and (10-12) facets accompanied the overall free energy barriers of 71.8 and 142.4 $\text{kJ}\cdot\text{mol}^{-1}$, respectively.

On the other hand, with respect to $\text{CH} + \text{CHO} + \text{H}$ species, as shown in Fig. 5(b), on fcc Rh(111), ethanol is the major product, which is also indirectly supported by Nørskov *et al.*'s experiment and DFT calculations (Yang *et al.*, 2016) that Rh(111) exhibits high selectivity toward acetaldehyde. On hcp Rh(10–10), methane and ethanol are the main products, methane reduces ethanol production. On hcp Rh(0001), acetylene is the dominant product, methane is competitive with ethanol. On hcp Rh(10–12) and fcc Rh(100), methane is the favored product, but the formation of ethylene or acetylene affects the yield of ethanol. These results are coinciding with the experimental results that methane or C_2+ hydrocarbons is the main product on Rh catalyst (Xie *et al.*, 2016; Glezakou *et al.*, 2012; Song *et al.*, 2012; Mei *et al.*, 2010; Chen *et al.*, 2016; Ding *et al.*, 2018). More importantly, according to the occupied proportion of different crystal facets in the hcp and fcc Rh crystal phases, compared to the hcp Rh catalysts, the fcc Rh catalyst has higher ethanol selectivity, especially, the dominantly exposed Rh(111) facet.

Starting from the CH_x monomer, except for Rh(111) facet, the selectivity of ethanol is lower than that of methane or C_2 hydrocarbons on the other four Rh facets. The microkinetic modeling results also show that Rh(111) exhibits the excellent selectivity toward ethanol formation, the formation rates of methane, methanol, acetylene and ethanol (see details in the Supplementary Material) are 7.14×10^{-19} , 2.62×10^{-21} , 1.71×10^{-17} and $2.39 \times 10^{-8} \text{ s}^{-1}$, respectively. The selectivity of ethanol over the fcc Rh(100) and hcp Rh(0001), (10–10), (10–12) facets is mainly controlled by methane and C_2 hydrocarbons formation. That is, the self-coupling and hydrogenation of CH_x and CHO with CH_x are the selectivity-controlled steps of ethanol formation on the fcc Rh and hcp Rh catalysts.

According to DFT calculations, two possible ways are proposed to increase the productivity of ethanol on Rh catalyst: one is to inhibit the formation of methane and C_2 hydrocarbons; the other is to accelerate CHO insertion into CH_x . Aiming at realizing above proposals, we need to get the help from metal promoter introduced into Rh catalyst to inhibit the coupling and hydrogenation of CH_x and/or promote CHO insertion into CH_x species. Several publications on the fcc Rh-based catalysts (Glezakou *et al.*, 2012; Yang *et al.*, 2017; Yang *et al.*, 2016; Yin *et al.*, 2003) have shown from

both experiments and theory that the dominant function of introducing a metal promoter is to inhibit the reactions of CH_x hydrogenation and CH_x coupling.

3.4. The effects of Rh crystal phase and facet in the Fe-modified Rh on C_2 oxygenates

As mentioned above, aiming at increasing ethanol productivity over Rh catalysts, we introduce the promoter Fe into Rh catalyst, which is known to be one of the promising promoters (Palomino *et al.*, 2015; Liu *et al.*, 2015; Carrillo *et al.*, 2018; Liu *et al.*, 2017); the results are expected to further clarify the effects of Rh crystal phase and facet in the metal promoter-modified Rh catalyst on the catalytic activity and selectivity of C_2 oxygenates formation. Starting from the CH monomer, the formation of methane, C_2 hydrocarbons and C_2 oxygenates over the Fe-modified Rh(111), (100), (0001), (10–10) and (10–12) facets are examined (see details in Figs. S22–S29). As presented in Fig. 6, the formation of methane and C_2 hydrocarbons is effectively inhibited on the Fe-modified Rh(111), (100) and (0001) facets, which exhibits excellent selectivity toward C_2 oxygenates. However, methane formation is preferred over C_2 hydrocarbons and C_2 oxygenates on the Fe-modified Rh(10–10) facet; the formation of methane and C_2 hydrocarbons is more favorable than that of C_2 oxygenates on Fe-modified Rh(10–12) facet. On the other hand, the activity order of C_2 oxygenates formation is $\text{FeRh}(100) > \text{FeRh}(111) > \text{FeRh}(0001) > \text{FeRh}(10-12) > \text{FeRh}(10-10)$ with the overall free energy barriers of 66.5, 85.0, 87.9, 121.7 and 144.6 $\text{kJ}\cdot\text{mol}^{-1}$, respectively. Further, among the FeRh(111), (100) and (0001) facets with better C_2 oxygenates selectivity, the Rh(0001) facet only covers 16.92% of the hcp Rh surface, meanwhile, the activity of C_2 oxygenates formation on FeRh(0001) facet is lower than that on the FeRh(111) and (100) facets.

In general, the promoter Fe has a slight promotion effect for the catalytic activity and selectivity improvement of C_2 oxygenates formation on the hcp Rh; whereas on the Rh(100) and (111) facets occupying 81.78% surface proportion of fcc Rh, the selectivity and activity of C_2 oxygenates formation is higher than that of three hcp Rh facets, which means that the promoter Fe significantly improve the catalytic performance of fcc Rh toward C_2 oxygenates

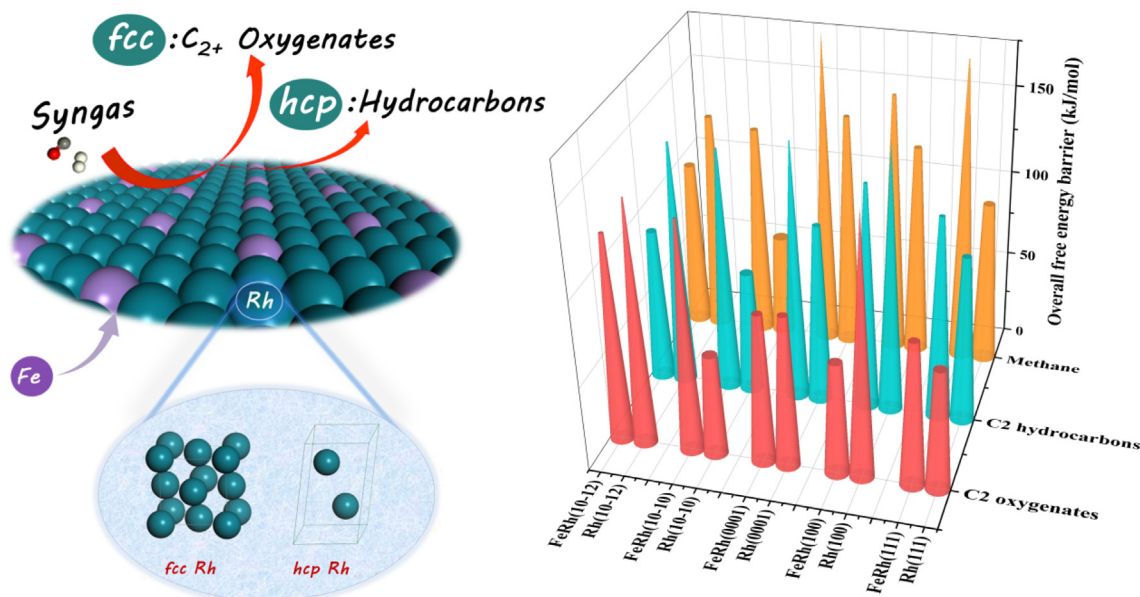


Fig. 6. The effect of Fe for the catalytic activity and selectivity of C_2 oxygenates formation on the fcc and hcp Rh crystal facet. The calculated overall free energy barriers of methane, C_2 hydrocarbons and C_2 oxygenates formation with respect to CH species on different Rh and Fe-modified Rh facets at 523 K are presented in Fig. S29.

formation. Therefore, the activity and selectivity of C₂ oxygenates formation on the Fe-modified Rh catalysts still depended on Rh crystal phase and facet, in which the effect of the promoter Fe into the fcc Rh is much superior to that into the hcp Rh. Meanwhile, this result also confirms that inhibiting the coupling and hydrogenation of CH_x and/or promoting CHO insertion into CH_x species can improve the productivity of ethanol on Rh catalyst by introducing metal promoters, especially, the fcc Rh catalysts.

Therefore, for CO hydrogenation to ethanol on the promoter-modified Rh-based catalyst, it should be focused on the fcc crystal phase instead of hcp crystal phase, especially the dominant exposed fcc Rh(111) facet, which not only highly-active catalyze CH formation and CHO reaction with CH_x to C₂ oxygenates, but also effectively inhibit methanol and hydrocarbons formation, leading to excellent production of ethanol. The findings in this work for the first time provide a fundamental understanding for the sensitivity of Rh crystal phase to catalyze CO hydrogenation to ethanol, and give out experimental clues for the design of high-performance Rh-based catalyst.

4. Conclusions

This study has systematically investigated the activity and selectivity of ethanol synthesis from syngas over different crystal facets of hcp Rh ((0001), (10–10), (10–12)) and fcc Rh ((100) and (111)) using DFT calculations with microkinetic modeling. The results identify the effects of Rh crystal phase and facet on the catalytic performance of ethanol formation from syngas. That is, compared to the hcp Rh, the fcc Rh can expose much denser active facets to present higher intrinsic activity of CH and ethanol formation. Moreover, compared to Ni, Ru, Co and Cu catalysts, the fcc Rh catalyst realizes a balance between CO/CHO dissociation into CH species and the undissociated CO/CHO species, which is significantly necessary for syngas conversion to ethanol. Further, the activity and selectivity of C₂ oxygenates formation over the Fe-modified Rh catalysts still depended on Rh crystal phase and facet, in which the effect of the promoter Fe into the fcc Rh is much superior to that into the hcp Rh. Therefore, Rh-based catalysts should be focused on fcc crystal phase instead of hcp crystal phase, ethanol productivity on the fcc Rh should be regulated by introducing metal promoter, which dominantly plays a role to inhibit the formation of hydrocarbons and/or promote the formation of C₂ oxygenates.

CRedit authorship contribution statement

Li Kang: Writing – original draft, Writing – review & editing, Formal analysis. **Yuan Zhang:** Writing – review & editing, Data curation, Formal analysis. **Lixuan Ma:** Formal analysis, Data curation. **Baojun Wang:** Writing – original draft, Writing – review & editing, Data curation, Conceptualization, Funding acquisition, Resources, Software, Project administration, Supervision. **Mao-hong Fan:** Formal analysis. **Debao Li:** Formal analysis. **Riguang Zhang:** Writing – original draft, Writing – review & editing, Data curation, Conceptualization, Funding acquisition, Resources, Project administration, Supervision.

Declaration of Competing Interest

The authors declare that they have no known competing financial interests or personal relationships that could have appeared to influence the work reported in this paper.

Acknowledgments

This work is financially supported by the Key projects of National Natural Science Foundation of China (No. 21736007), the National Natural Science Foundation of China (No. 21776193), the Top Young Innovative Talents of Shanxi.

Appendix A. Supplementary material

Supplementary data to this article can be found online at <https://doi.org/10.1016/j.ces.2021.117186>.

References

- Farrell, A.E.R., Plevin, J., Turner, B.T., Jones, A.D., 2006. M. ÓHare, D.M. Kammen, Ethanol can contribute to energy and environmental goals. *Science* 311, 506–508.
- Pan, X.L., Fan, Z.L., Chen, W., Ding, Y.J., Luo, H.Y., Bao, X.H., 2007. Enhanced ethanol production inside carbon-nanotube reactors containing catalytic particles. *Nat. Mater.* 6, 507–511.
- An, B., Li, Z., Song, Y., Zhang, J., Zeng, L., Wang, C., Lin, W., 2019. Cooperative copper centres in a metal–organic framework for selective conversion of CO₂ to ethanol. *Nat. Commun.* 2, 709–717.
- Yang, C.S., Mu, R., Wang, G.S., Song, J.M., Tian, H., Zhao, Z.J., Gong, J.L., 2019. Hydroxyl-mediated ethanol selectivity of CO₂ hydrogenation. *Chem. Sci.* 10, 3161–3167.
- Song, Y.F., Chen, W., Zhao, C.C., Li, S.G., Wei, W., Sun, Y.H., 2017. Metal-free nitrogen-doped mesoporous carbon for electroreduction of CO₂ to ethanol. *Angew. Chem.* 56, 10840–10844.
- Spivey, J.J., Egbeki, A., 2007. Heterogeneous catalytic synthesis of ethanol from biomass-derived syngas. *Chem. Soc. Rev.* 36, 1514–1528.
- Subramani, V., Gangwal, S.K., 2008. A review of recent literature to search for an efficient catalytic process for the conversion of syngas to ethanol. *Energy Fuels* 22, 814–839.
- Luk, H.T., Mondelli, C., Ferré, D.C., Stewart, J.A., Pérez-Ramírez, J., 2017. Status and prospects in higher alcohols synthesis from syngas. *Chem. Soc. Rev.* 46, 1358–1426.
- Liu, J.J., Tao, R.Z., Guo, Z., Regalbutto, J.R., Marshall, C.L., Klie, R.F., Miller, J.T., Meyer, R. J., 2013. Selective adsorption of manganese onto rhodium for optimized Mn/Rh/SiO₂ alcohol synthesis catalysts. *ChemCatChem* 5, 3665–3672.
- Xie, Z.L., Frank, B., Huang, X., Schlögl, R., Trunschke, A., 2016. Higher alcohol synthesis over Rh catalysts: conditioning of Rh/N-CNTs by Co and Mn entrapped in the support. *Catal. Lett.* 146, 2417–2424.
- Glezakou, V.A., Jaffe, J.E., Rousseau, R., Mei, D.H., Kathmann, S.M., Albrecht, K.O., Gray, M.J., Gerber, M.A., 2012. The role of Ir in ternary Rh-based catalysts for syngas conversion to C₂ oxygenates. *Top Catal.* 55, 595–600.
- Schwartz, V., Campos, A., Egbeki, A., Spivey, J.J., Overbury, S.H., 2011. EXAFS and FT-IR characterization of Mn and Li promoted titania-supported Rh catalysts for CO hydrogenation. *ACS Catal.* 1, 1298–1306.
- Yang, N.Y., Liu, X.Y., Asundi, A.S., Nørskov, J.K., Bent, S.F., 2018. The role of sodium in tuning product distribution in syngas conversion by Rh catalysts. *Catal. Lett.* 148, 289–297.
- Xu, D.D., Zhang, H.T., Ma, H.F., Qian, W.X., Ying, W.Y., 2017. Effect of Ce promoter on Rh-Fe/TiO₂ catalysts for ethanol synthesis from syngas. *Catal. Commun.* 98, 90–93.
- Liu, W.G., Wang, S., Wang, S.D., 2016. Effect of impregnation sequence of Ce promoter on the microstructure and performance of Ce-promoted Rh-Fe/SiO₂ for the ethanol synthesis. *Appl. Catal. A: Gen.* 510, 227–232.
- Yang, N.Y., Yoo, J.S., Schumann, J., Bothra, P., Singh, J.A., Valle, E., Pedersen, F.A., Nørskov, J.K., Bent, S.F., 2017. Rh-MnO interface sites formed by atomic layer deposition promote syngas conversion to higher oxygenates. *ACS Catal.* 7, 5746–5757.
- Song, X.G., Ding, Y.J., Chen, W.M., Dong, W.D., Pei, Y.P., Zang, J., Yan, L., Lu, Y., 2012. Bimetal modified ordered mesoporous carbon as a support of Rh catalyst for ethanol synthesis from syngas. *Catal. Commun.* 19, 100–104.
- Li, F.Y., Jiang, D.E., Zeng, X.C., Chen, Z.F., 2012. Mn monolayer modified Rh for syngas-to-ethanol conversion: a first-principles study. *Nanoscale* 4, 1123–1129.
- Mei, D.H., Rousseau, R., Kathmann, S.M., Glezakou, V.A., Engelhard, M.H., Jiang, W.L., Wang, C.M., Gerber, M.A., White, J.F., Stevens, D.J., 2010. Ethanol synthesis from syngas over Rh-based/SiO₂ catalysts: a combined experimental and theoretical modeling study. *J. Catal.* 271, 325–342.
- Choi, Y., Liu, P., 2009. Mechanism of ethanol synthesis from syngas on Rh(111). *J. Am. Chem. Soc.* 131, 13054–13061.
- Wang, J.C., Liu, Z.X., Zhang, R.G., Wang, B.J., 2014. Ethanol synthesis from syngas on the stepped Rh(211) surface: effect of surface structure and composition. *J. Phys. Chem. C* 118, 22691–22701.
- Liu, Jin-Xun, Zhang, Bing-Yan, Chen, Pei-Pei, Su, Hai-Yan, Li, Wei-Xue, 2016. CO dissociation on face-centered cubic and hexagonal close-packed nickel catalysts: a first-principles study. *J. Phys. Chem. C* 120 (43), 24895–24903.
- Li, W.Z., Liu, J.X., Gu, J., Zhou, W., Yao, S.Y., Si, R., Guo, Y., Su, H.Y., Yan, C.H., Li, W.X., Zhang, Y.W., Ma, D., 2017. Chemical insights into the design and development of

- face-centered cubic ruthenium catalysts for Fischer-Tropsch synthesis. *J. Am. Chem. Soc.* 139, 2267–2276.
- Liu, Jin-Xun, Su, Hai-Yan, Sun, Da-Peng, Zhang, Bing-Yan, Li, Wei-Xue, 2013. Crystallographic dependence of CO activation on cobalt catalysts: HCP versus FCC. *J. Am. Chem. Soc.* 135 (44), 16284–16287.
- Huang, J.L., Li, Z., Duan, H.H., Cheng, Z.Y., Li, Y.D., Zhu, J., Yu, R., 2017. Formation of Hexagonal-Close Packed (HCP) rhodium as a size effect. *J. Am. Chem. Soc.* 139, 575–578.
- Zhang, R.G., Kang, L., Liu, H.X., Wang, B.J., Li, D.B., Fan, M.H., 2020. Crystal facet dependence of carbon chain growth mechanism over the Hcp and Fcc Co catalysts in the Fischer-Tropsch synthesis. *Appl. Catal. B: Environ.* 269, 118847.
- Kusada, K., Kitagawa, H., 2016. A route for phase control in metal nanoparticles: a potential strategy to create advanced materials. *Adv. Mater.* 28, 1129–1142.
- Liu, Jin-Xun, Li, Wei-Xue, 2016. Theoretical study of crystal phase effect in heterogeneous catalysis. *WIREs Interdiscip. Rev.: Comput. Mol. Sci.* 6 (5), 571–583.
- Yang, L., Liu, P., 2014. Ethanol synthesis from syngas on transition metal-doped Rh (111) surfaces: a density functional kinetic monte carlo study. *Top. Catal.* 57, 125–134.
- Yang, N.Y., Medford, A.J., Liu, X.Y., Studt, F., Bligaard, T., Bent, S.F., Nørskov, J.K., 2016. Intrinsic selectivity and structure sensitivity of rhodium catalysts for C₂₊ oxygenate production. *J. Am. Chem. Soc.* 138, 3705–3714.
- Kapur, N., Hyun, J., Shan, B., Nicholas, J.B., Cho, K., 2010. Ab initio study of CO hydrogenation to oxygenates on reduced Rh terraces and stepped surfaces. *J. Phys. Chem. C* 114, 10171–10182.
- Medford, A.J., Lausche, A.C., Pedersen, F.A., Temel, B., Schjødt, N.C., Nørskov, J.K., Studt, F., 2014. Activity and selectivity trends in synthesis gas conversion to higher alcohols. *Top. Catal.* 57, 135–142.
- Kitakami, O., Sato, H., Shimada, Y., Sato, F., Tanaka, M., 1997. Size effect on the crystal phase of cobalt fine particles. *Phys. Rev. B* 56, 13849–13854.
- Fan, Z., Zhang, H., 2016. Crystal phase-controlled synthesis, properties and applications of noble metal nanomaterials. *Chem. Soc. Rev.* 45, 63–82.
- Braconnier, L., Landrivo, E., 2013. I. Cléménçon, C. Legens, F. Diehl, Y. Schuurman, How does activation affect the cobalt crystallographic structure? An in situ XRD and magnetic study. *Catal. Today* 215, 18–23.
- Prieto, G., 2013. P. Concepción, R. Murciano, A. Martínez, The impact of pre-reduction thermal history on the metal surface topology and site-catalytic activity of Co/SiO₂ Fischer-Tropsch catalysts. *J. Catal.* 302, 37–48.
- Koster, A., Santen, R.A., 1990. Dissociation of CO on Rh surfaces. *Surf. Sci.* 233, 366–380.
- Filot, I.A.W., Shetty, S., Hensen, E.J.M., Santen, R.A., 2011. Size and topological effects of rhodium surfaces, clusters and nanoparticles on the dissociation of CO. *J. Phys. Chem. C* 115, 14204–14212.
- Asundi, A.S., Hoffman, A.S., Bothra, P., Boubnov, A., Vila, F.D., Yang, N., Singh, J.A., Zeng, L., Raiford, J.A., Abild-Pedersen, F., Bare, S.R., Bent, S.F., 2019. Understanding structure-property relationships of MoO₃-promoted Rh catalysts for syngas conversion to alcohols. *J. Am. Chem. Soc.* 141, 19655–19668.
- Gu, T., Wang, B., Chen, S., Yang, B., 2020. Automated generation and analysis of the complex catalytic reaction network of ethanol synthesis from syngas on Rh (111). *ACS Catal.* 10, 6346–6355.
- Furthmüller, J., Hafner, J., Kresse, G., 1996. Efficient iterative schemes for ab initio total-energy calculations using a plane-wave basis set. *Phys. Rev. B: Condens. Matter Mater. Phys.* 54, 11169–11186.
- Kresse, G., Furthmüller, J., 1996. Efficiency of ab-initio total energy calculations for metals and semiconductors using a plane-wave basis set. *Comput. Mater. Sci.* 6, 15–50.
- Perdew, J.P., Burke, K., Ernzerhof, M., 1996. Generalized gradient approximation made simple. *Phys. Rev. Lett.* 77, 3865–3868.
- Henkelman, G., Uberuaga, B.P., Jónsson, H., 2000. A climbing image nudged elastic band method for finding saddle points and minimum energy paths. *J. Chem. Phys.* 113, 9901–9904.
- Henkelman, G., Jónsson, H., 2000. Improved tangent estimate in the nudged elastic band method for finding minimum energy paths and saddle points. *J. Chem. Phys.* 113, 9978–9985.
- Henkelman, G., Jónsson, H., 1999. A dimer method for finding saddle points on high dimensional potential surfaces using only first derivatives. *J. Chem. Phys.* 111, 7010–7022.
- Yin, H.M., Ding, Y.J., Luo, H.Y., Yan, L., Wang, T., Lin, L.W., 2003. The performance of C₂ oxygenates synthesis from syngas over Rh-Mn-Li-Fe/SiO₂ catalysts with various Rh loadings. *Energy Fuels* 17, 1401–1406.
- Zuo, Z.J., Wang, L., Yu, L.M., Han, P.D., Huang, W., 2014. Experimental and theoretical studies of ethanol synthesis from syngas over CuZnAl catalysts without other promoters. *J. Phys. Chem. C* 118, 12890–12898.
- Zhao, Y.H., Sun, K.J., Ma, X.F., Liu, J.X., Sun, D.P., Su, H.Y., Li, W.X., 2011. Carbon chain growth by formyl insertion on rhodium and cobalt catalysts in syngas conversion. *Angew. Chem.* 123, 5447–5450.
- Zhang, R.G., Wang, G.R., Wang, B.J., Ling, L.X., 2014. Insight into the effect of promoter Mn on ethanol formation from syngas on a Mn-promoted MnCu(211) surface: a comparison with a Cu(211) surface. *J. Phys. Chem. C* 118, 5243–5254.
- Zhang, R.G., Wang, G.R., Wang, B.J., 2013. Insights into the mechanism of ethanol formation from syngas on Cu and an expanded prediction of improved Cu-based catalyst. *J. Catal.* 305, 238–255.
- Wang, Wei, Wang, Ye, Wang, Gui-Chang, 2018. Ethanol synthesis from syngas over Cu(Pd)-doped Fe(100): a systematic theoretical investigation. *Phys. Chem. Chem. Phys.* 20 (4), 2492–2507.
- Zhang, R.G., Sun, X.C., Wang, B.J., 2013. Insight into the preference mechanism of CH_x (x=1-3) and C-C chain formation involved in C₂ oxygenate formation from syngas on the Cu(110) surface. *J. Phys. Chem. C* 117, 6594–6606.
- Zheng, H.Y., Zhang, R.G., Li, Z., Wang, B.J., 2015. Insight into the mechanism and possibility of ethanol formation from syngas on Cu(100) surface. *J. Mol. Catal. A: Chem.* 404–405, 115–130.
- Lausche, A.C., Medford, A.J., Khan, T.S., Xu, Y., Bligaard, T., Abild-Pedersen, F., Nørskov, J.K., Studt, F., 2013. On the effect of coverage dependent adsorbate-adsorbate interactions for CO methanation on transition metal surfaces. *J. Catal.* 307, 275–282.
- Yao, Z., Guo, C., Mao, Y., Hu, P., 2019. Quantitative determination of C-C coupling mechanisms and detailed analyses on the activity and selectivity for Fischer-Tropsch synthesis on Co(0001): microkinetic modeling with coverage effects. *ACS Catal.* 9, 5957–5973.
- Li, L., Sholl, D.S., 2015. Computational identification of descriptors for selectivity in syngas reactions on a Mo₂C catalyst. *ACS Catal.* 5, 5174–5185.
- Van Belleghem, J., Ledesma, C., Yang, J., Toch, K., Chen, D., Thybaut, J.W., Marin, G.B., 2016. A single-event microkinetic model for the cobalt catalyzed Fischer-Tropsch synthesis. *Appl. Catal. A: Gen.* 524, 149–162.
- Stegelmann, C., Andreasen, A., Campbell, C.T., 2009. Degree of rate control: how much the energies of intermediates and transition states control rates. *J. Am. Chem. Soc.* 131, 8077–8082.
- Kozuch, S., Shaik, S., 2006. A combined kinetic-quantum mechanical model for assessment of catalytic cycles: application to cross-coupling and Heck reactions. *J. Am. Chem. Soc.* 128, 3355–3365.
- Wang, W.Y., Wang, G.C., 2021. The first-principles-based microkinetic simulation of the dry reforming of methane over Ru(0001). *Catal. Sci. Technol.* 11, 1395–1406.
- Zhi, Cuimei, Wang, Qiang, Wang, Baojun, Li, Debao, Zhang, Riguang, 2015. Insight into the mechanism of methane synthesis from syngas on a Ni(111) surface: a theoretical study. *RSC Adv.* 5 (82), 66742–66756.
- Zhi, C.M., Zhang, R.G., Wang, B.J., 2017. Comparative studies about CO methanation over Ni(211) and Zr-modified Ni(211) surfaces: qualitative insight into the effect of surface structure and composition. *Mol. Catal.* 438, 1–14.
- Liu, Z.P., Hu, P., 2002. A new insight into Fischer-Tropsch synthesis. *J. Am. Chem. Soc.* 124, 11568–11569.
- Filot, I.A.W., van Santen, R.A., Hensen, E.J.M., 2014. Quantum chemistry of the Fischer-Tropsch reaction catalysed by a stepped ruthenium surface. *Catal. Sci. Technol.* 4, 3129–3140.
- Zhang, R.G., Liu, F., Wang, Q., Wang, B.J., Li, D.B., 2016. Insight into CH_x formation in Fischer-Tropsch synthesis on the hexahedron Co catalyst: effect of surface structure on the preferential mechanism and existence form. *Appl. Catal. A: Gen.* 525, 76–84.
- Wen, Guangxiang, Wang, Qiang, Zhang, Riguang, Li, Debao, Wang, Baojun, 2016. Insight into the mechanism about the initiation, growth and termination of the C-C chain in syngas conversion on the Co(0001) surface: a theoretical study. *Phys. Chem. Chem. Phys.* 18 (39), 27272–27283.
- Chen, Congbiao, Wang, Qiang, Wang, Guiru, Hou, Bo, Jia, Litao, Li, Debao, 2016. Mechanistic insight into the C₂ hydrocarbons formation from syngas on Fcc-Co (111) surface: a DFT study. *J. Phys. Chem. C* 120 (17), 9132–9147.
- Van Santen, R.A., Neurock, M., 1995. Concepts in Theoretical heterogeneous catalytic reactivity. *Catal. Rev.-Sci. Eng.* 37, 557–698.
- Hammer, B., Nørskov, J.K., 2000. Theoretical surface science and catalysis-calculations and concepts. *Adv. Catal.* 45, 71–129.
- Chen, W.M., Ding, Y.J., Xue, F., Song, X.G., Ning, L.L., 2016. Highly efficient β-SiC-supported 0.5% Rh-based catalyst for CO hydrogenation to C₂ oxygenates. *Catal. Commun.* 85, 44–47.
- Ding, Dan, Yu, Jun, Guo, Qiangsheng, Guo, Xiaoming, Mao, Haifang, Mao, Dongsun, 2018. Highly efficient synthesis of C₂ oxygenates from CO hydrogenation over Rh-Mn-Li/SiO₂ catalyst: the effect of TiO₂ promoter. *Catal. Lett.* 148 (8), 2619–2626.
- Palomino, R.M., Magee, J.W., Llorca, J., Senanayake, S.D., White, M.G., 2015. The effect of Fe-Rh alloying on CO hydrogenation to C₂₊ oxygenates. *J. Catal.* 329, 87–94.
- Liu, W.G., Wang, S., Sun, T.J., Wang, S.D., 2015. The promoting effect of Fe doping on Rh/CeO₂ for the ethanol synthesis. *Catal. Lett.* 145, 1741–1749.
- Carrillo, P., Shi, R., Teeluck, K., Senanayake, S.D., White, M.G., 2018. In situ formation of FeRh nanoalloys for oxygenate synthesis. *ACS Catal.* 8, 7279–7286.
- Liu, Y.F., Göeltl, F., Ro, I., Ball, M.R., Sener, C., Aragão, I.B., Zanchet, D., Huber, G.W., Mavrikakis, M., Dumesic, J.A., 2017. Synthesis gas conversion over Rh-based catalysts promoted by Fe and Mn. *ACS Catal.* 7, 4550–4563.